Journal of Environmental Radioactivity 138 (2014) 50–59

Contents lists available at ScienceDirect

Journal of Environmental Radioactivity

journal homepage: www.elsevier.com/locate/jenvrad

Development and comparison of computational models for estimation of absorbed organ radiation dose in rainbow trout (*Oncorhynchus mykiss*) from uptake of iodine-131

N.E. Martinez [a, *], T.E. Johnson [b], K. Capello [c], J.E. Pinder III [b]

[a] Department of Environmental Engineering and Earth Sciences, Clemson University, 342 Computer Ct, Anderson, SC 29625, USA
[b] Department of Environmental and Radiological Health Sciences, Colorado State University, 1681 Campus Delivery, Fort Collins, CO 80523, USA
[c] Human Monitoring Laboratory, National Internal Radiation Assessment Section, Radiation Protection Bureau, 775 Brookfield Road, Ottawa, Ontario K1A 1C1, Canada

ARTICLE INFO

Article history:
Received 7 April 2014
Received in revised form
30 July 2014
Accepted 3 August 2014
Available online 26 August 2014

Keywords:
Radiation dosimetry
Monte Carlo
Iodine-131
Rainbow trout

ABSTRACT

This study develops and compares different, increasingly detailed anatomical phantoms for rainbow trout (*Oncorhynchus mykiss*) for the purpose of estimating organ absorbed radiation dose and dose rates from ^{131}I uptake in multiple organs. The models considered are: a simplistic geometry considering a single organ, a more specific geometry employing additional organs with anatomically relevant size and location, and voxel reconstruction of internal anatomy obtained from CT imaging (referred to as CSUTROUT). Dose Conversion Factors (DCFs) for whole body as well as selected organs of *O. mykiss* were computed using Monte Carlo modeling, and combined with estimated activity concentrations, to approximate dose rates and ultimately determine cumulative radiation dose (μGy) to selected organs after several half-lives of ^{131}I. The different computational models provided similar results, especially for source organs (less than 30% difference between estimated doses), and whole body DCFs for each model (~3×10^{-3} μGy d^{-1} per Bq kg^{-1}) were comparable to DCFs listed in ICRP 108 for ^{131}I. The main benefit provided by the computational models developed here is the ability to accurately determine organ dose. A conservative mass-ratio approach may provide reasonable results for sufficiently large organs, but is only applicable to individual source organs. Although CSUTROUT is the more anatomically realistic phantom, it required much more resource dedication to develop and is less flexible than the stylized phantom for similar results. There may be instances where a detailed phantom such as CSUTROUT is appropriate, but generally the stylized phantom appears to be the best choice for an ideal balance between accuracy and resource requirements.

1. Introduction

1.1. Current methodology in radiation protection of the environment

Radiation dose rates to biota are typically approximated utilizing dose conversion factors (DCF), which are values for absorbed dose rate per unit activity concentration in the body or organ (i.e. mGy d^{-1} per Bq g^{-1}). The current methodology employed by both the ICRP (International Commission on Radiological Protection) and the ERICA Integrated Approach (Larsson, 2008) for calculating dose conversion coefficients employs Monte Carlo modeling of a uniformly distributed radionuclide within an ellipsoidal phantom designed to represent hypothetical organisms (ICRP, 2008; Gómez-Ros et al., 2008). For example, ICRP 108 includes a reference trout (1.26 kg, 50 cm long) that in principle could represent any freshwater fish with similar dimensions (ICRP, 2008).

It has been shown that when computing whole-body DCF, the assumption of a homogenous distribution will result in an uncertainty of less than 30% for both electrons and photons when comparing to a monoenergetic point source at the center or periphery of the ellipsoid (which gives the range of possible DCFs) (Gómez-Ros et al., 2008). However, if a radionuclide is not homogeneously distributed but instead concentrates in a particular organ (e.g. iodine-131 in the thyroid) a much higher dose will be received by the organ or tissue than by the whole body. Organs have been generically modeled as spheres within the whole-body ellipsoid phantom to address situations where nuclides

* Corresponding author. Tel.: +1 864 656.1984.
E-mail address: nmarti3@clemson.edu (N.E. Martinez).

http://dx.doi.org/10.1016/j.jenvrad.2014.08.001
0265-931X/

concentrate in an organ, (ICRP, 2008), but this simplicity may be insufficient to accurately represent the complex and variable nature of organ structure and arrangement within different types of organisms. The ratio of whole-body to organ mass offers a conservative conversion of whole-body to organ dose, but may be a considerable overestimate (Gómez-Ros et al., 2008). More accurate estimates of organ dose can be made by combining activity concentration data with direct Monte Carlo calculations of energy deposition in individual organs.

1.2. Study objective and justification

Establishment of appropriate screening levels in the regulatory paradigm requires incorporation of sufficient knowledge of dose effects; the ICRP currently lists no derived consideration reference levels for organs, meaning that specific risks associated with organ dose rates are unavailable (ICRP, 2008). Although it is known that radioiodine exposures can negatively affect certain aspects of fish growth and development mediated by thyroidal hormones (La Roche et al., 1965, 1966), no information is currently available linking risk of occurrence to thyroid radiation dose levels associated with ^{131}I exposure. Relating effects to dose levels requires either a direct determination of dose or a modelling methodology for dose approximation. Accuracy is important in dose-effects studies; relating an effect to an underestimate of dose (or dose rate) may result in unnecessary and expensive remediation efforts. Conversely, if the dose (or dose rate) required to cause an effect is overestimated, regulatory bodies may establish environmental protection standards at levels not adequately protective (Ruedig et al., 2014).

Since the ICRP's recommendations in 2008, radiation protection in the environmental setting has focused on limiting adverse population effects (ICRP, 2008); i.e., dose limits are established to protect against such endpoints as population decline. However, dose levels at which effects are seen across individuals can lead to an effect on the population. For example, a decline in reproductive success or absence of sexual development (such as resulting from a significant exposure to ^{131}I; La Roche et al., 1966) in individual trout could lead to a decline in trout population. Therefore, the models presented and discussed here have relevancy beyond dose determination and protection of the individual.

Improved dosimetric methods will enable the ability to relate dose to effects and subsequently determine risk from exposure to radiation. Model comparison and refinement is important to the process of determining dose rates, doses, and dose effects. Here we develop and compare three models for rainbow trout (*Oncorhynchus mykiss*): (1) a simplistic geometry considering a single organ, (2) a more specific geometry including multiple organs of anatomically relevant size and location, and (3) voxel reconstruction of internal anatomy obtained from CT imaging. We determine the doses and dose rates to various organs from uptake and accumulation of ^{131}I in thyroid, GI tract, and liver of rainbow trout, where the time-varying concentrations of ^{131}I in these organs were determined for the first 32 days following an ^{131}I release into the freshwater system (Martinez et al., 2014). Iodine-131 is a major component of the atmospheric releases following reactor accidents, and although the fate of ^{131}I deposition onto lakes and other aquatic systems has been studied considerably (e.g. Bird et al., 1995a, 1995b; Bird and Schwartz, 1996; Gilfedder et al., 2009, 2010), the resulting doses to aquatic organisms have received less attention. The goal of this study is to determine the differences between increasingly true-to-life models in predicting radiation dose to biota. Computational phantoms have found extensive use through incorporation into Monte Carlo based radiation transport computer codes for application in radiation dosimetry, as well as in medical imaging simulation and evaluation (Zaidi and Tsui, 2009; Xu and Eckerman, 2010). A significant amount of research has been conducted concerning human model development, however work conducted in creating animal models is lacking (Zaidi and Tsui, 2009). The initial research and subsequent increase in animal model development over the past decade was motivated by the need for refined preclinical models, and therefore initially focused on laboratory animals (Zaidi and Tsui, 2009). In recent years, there has been increased emphasis on radiation protection of the environment, and some models have been used for this specific end (Mohammadi et al., 2011, 2012; Caffrey and Higley, 2013; Ruedig et al., 2014). The reader is directed to the supplementary online material for a listing of existing whole body animal phantoms, along with studies that have calculated absorbed fractions or organ dose coefficients using such phantoms (Hindorf et al., 2004; Segars et al., 2004; Stabin et al., 2006; Taschereau et al., 2006; Bitar et al., 2007; Dogdas et al., 2007; Kinase, 2008; Padilla et al., 2008; Wu et al., 2008; Xie et al., 2010a, 2010b; Zhang et al., 2009, 2012; Mohammadi et al., 2011, 2012; Kramer et al., 2012; Caffery and Higley, 2013; Mauxion et al., 2013; Ruedig et al., 2014).

A study similar to ours compared absorbed fractions determined by three different computational phantoms for rat (Xie et al., 2010a) and found that the stylized phantom might underestimate organ dose. Additionally, Ruedig et al. (2014) found general agreement between voxel-based DCFs and the current DCFs recommended by the ICRP for trout for a variety of photon and electron energies. However, ours is the first study to consider temporal changes in activity concentration data as applied to organ uptake in various phantom types (namely, two stylized phantoms and one voxel phantom). Specific objectives of this study include:

(1) Describe and apply a methodology for approximating absorbed radiation dose and dose rates to the whole body and selected organs of the rainbow trout:
   (a) Create empirical models for predicting temporal activity concentrations in the rainbow trout thyroid, liver, and gastrointestinal tract based on existing kinetic data for ^{131}I;
   (b) Create anthropomorphic models for rainbow trout and combining them with empirical models for activity concentration to determine doses and dose rates;
(2) Compare the created anthropomorphic models and discuss the benefits and drawbacks of each;
(3) Compare anthropomorphic models to the traditional mass ratio approach in calculating DCF;
(4) Briefly consider the effect of fish size on results;
(5) Discuss the utility and implications of improved dosimetric methodology.

2. Materials and methods

2.1. Kinetic data for ^{131}I

Computing an accumulated radiation dose for time-varying organ concentrations requires some form of equation or model that describes the temporal concentration and location of the particular radionuclide. Martinez et al. (2014) used existing ^{131}I kinetic data (Short et al., 1969) from Fern Lake, Washington to develop empirically-derived models for the prediction of activity concentration in rainbow trout as well as various biota in the food web. We review the model development process here; for a detailed description and discussion we refer the reader to Martinez et al. (2014).

Fern Lake is a 9.7×10^4 m^2 oligotrophic lake near Seattle, Washington in the United States. The Fern Lake Trace Mineral

Metabolism program was a 10-year interdisciplinary research program initiated in 1957 (Donaldson et al., 1959) seeking to improve the productivity of western Washington lakes (Olsen et al., 1967). As part of the Fern Lake program, several radionuclides, including ^{131}I, were released into the lake to understand the fate and transport of the corresponding stable isotopes (e.g. ^{127}I) (Short et al., 1969, 1971). Iodine-131 concentrations in water, various biota, and trout tissues were measured periodically for 27 days, which is the data considered by Martinez et al. (2014). The following simple uptake and loss rate model was used to model the time varying concentrations of ^{131}I in fish tissues:

$$\frac{dB(t)}{dt} = \mu \cdot W(t) - k \cdot B(t) \quad (1)$$

where μ is an uptake constant with units L kg^{-1} d^{-1}, k is a first-order loss rate constant with units d^{-1}, $W(t)$ is the ^{131}I concentration in water, and $B(t)$ is the ^{131}I concentration in specific fish tissues. $W(t)$ is approximated using a single-component exponential equation (Whicker and Shultz, 1982):

$$W(t) = a \cdot e^{-bt} \quad (2)$$

where a is the initial ^{131}I concentration in the water at the time of release (*i.e.*, $t = 0$), and b is the rate constant (d^{-1}) for the exponential decline in $W(t)$. The solution to equation (1) is given by:

$$B(t) = \mu\left(\frac{a}{k-b}\right)\left(e^{-bt} - e^{-kt}\right) \quad (3)$$

For aquatic animal biota, μ is a measure of the transfer of the radionuclide through food chain pathways from the water to animal. The factors affecting μ become increasingly complex with increasing number of trophic levels (Pinder et al., 2009). Despite the number of factors affecting μ for consumers, the model has been shown to be able to accommodate these complexities for varying trophic levels (Smith et al., 2002; Pinder et al., 2011). When the model is applied to individual fish tissues, μ represents increases in ^{131}I concentrations due to absorption and ingestion of additional ^{131}I or to the transfer of ^{131}I from other tissues. For whole-body ^{131}I concentrations, k is a measure of loss that incorporates radioactive decay, excretion, and population losses due to mortality or emigration (Pinder et al., 2009). Population losses should be negligible for the studies considered here (short duration studies performed in mostly confined locations), so the estimated whole body k should be dominated by radionuclide decay and excretion. In addition to decay and excretion losses, k includes transfer to other tissues when applied to individual fish tissues.

Table 1 lists the specific values used for μ and k determined by Martinez et al. (2014), and Fig. 1 shows model fits compared to the Fern Lake data (Short et al., 1969; Martinez et al., 2014). The maintenance of nearly constant ^{131}I concentrations in the thyroid, GI tract, and liver is due to the continuing ingestion of ^{131}I from the trout's prey item components of the complex food web of Fern Lake.

Note that "thyroid" here refers to the biologically significant portion of the thyroid, or the thyroid epithelial shell (Martinez et al., 2014), and values for thyroid μ and k refer to samples of the

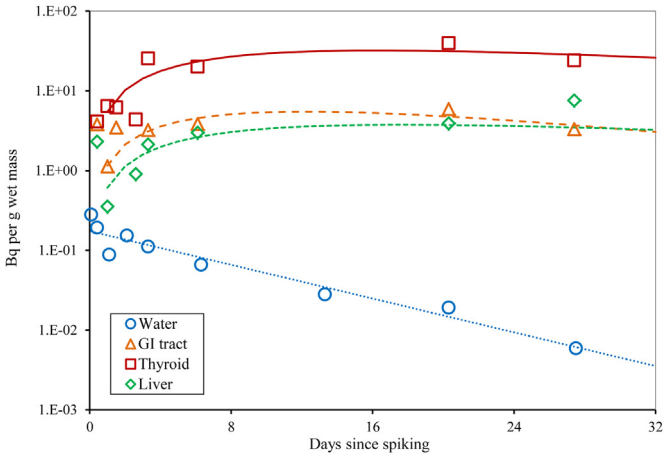

Fig. 1. Empirical model fits to ^{131}I concentrations in Fern Lake *O. mykiss* tissues. A comparison of Fern Lake data and model predictions for activity concentrations in water and *O. mykiss* thyroid, liver, and the gastrointestinal tracts.

"thyroid area" and may be underestimates of actual ^{131}I in the thyroid (Short et al., 1969; Martinez et al., 2014). Although variations among lakes in water temperature, stable iodine content, food chain complexity, fish size, and other factors may affect the values of μ and k, the Fern Lake values are the only available estimates of ^{131}I accumulation and loss in free-swimming fish, and are used here to calculate and compare organ radiation doses with various rainbow trout phantoms.

2.2. Analysis of fish anatomy

A 0.286 m long female *Oncorhynchus mykiss*, acquired from the Poudre River in Northern Colorado, was donated by a local fisherman for use in phantom development. The fish was CT scanned at the James L. Voss Veterinary Teaching Hospital in Fort Collins, Colorado[1] to acquire the image set necessary for phantom development. The DICOM files from the fish CT were imported into 3D-Doctor software,[2] and organs were outlined (contoured) manually in 3D-Doctor. The fish was dissected after CT to assist in appropriately identifying organs (Weinreb and Bilstad, 1955).

2.3. Phantom creation

The geometric structure, arrangement, and composition of rainbow trout tissues were either modelled (1) with organs represented as simple geometric shapes or (2) using Voxelizer[3] software. Voxelizer converts an organ boundary file, which is a set of organ contours created from CT images, into a lattice structure geometry (Kramer et al., 2010) recognizable by the Monte Carlo N-particle (MCNP) transport code[4] (X-5 Monte Carlo Team, 2003). MCNP was employed for Monte Carlo simulation of radiation transport in all models.

Because appropriate elemental composition data for trout tissue are as of yet unavailable, elemental compositions of tissues in all three models were based on human tissue (ICRU, 1989). This is

Table 1
Values for empirical parameters used in determination of activity concentration.

Source organ	μ (L kg^{-1} d^{-1})	k (d^{-1})
Thyroid	33.95	0.0276
Liver	3.76	0.0201
GI	7.25	0.0520

[1] 1 mm slices; Gemini TruFlight Big Bore PET/CT, Philips Healthcare, Andover, MA.
[2] Version 5.0, AbleSoftware Corp, Lexington, MA.
[3] Developed by the Human Monitoring Laboratory (HML), Health Canada, Ottawa.
[4] Version 5.1.60 or System X version 7.0D, known as MCNP5 and MCNPX respectively (Radiation Safety Information Computational Centre, Oak Ridge, TN).

consistent with previous work (Martinez et al., 2014; Kramer et al., 2012; Caffrey and Higley, 2013; Ruedig et al., 2014). The exception is the swim bladder, which was assumed to contain air. It should be noted that although there is existing data (e.g. Diem and Lentner, 1970) on trout tissue composition from a nutritional standpoint, it is not sufficiently specific for use in MCNP.

2.3.1. The simplistic phantom

The simplest phantom developed consists of an ellipsoidal fish body containing a thyroid modeled as 18 small cylindrical shells, based on rainbow trout thyroid anatomy (Raine et al., 2005). A complete description of the simple phantom is described by Martinez et al. (2014). The simple phantom was rescaled to match the size of the scanned fish. The height and width of the body were slightly reduced from the 9:2:1 (length:height:width) ratios utilized in Martinez et al. (2014) in order to fully match the dimensions of the aforementioned fish. We include the simplistic phantom in this study in addition to the stylized model described below, to determine if, when compared to uniform body composition, the presence of additional organs with varying densities and composition affect the dose to the thyroid.

2.3.2. Stylized phantom

A more detailed anatomical phantom was developed from the simplistic phantom; the size, shape, location, and composition of the fish body and thyroid are the same as for the simplistic phantom. Additional stylized organs, including the liver, swim bladder, gastrointestinal tract, ovaries, heart, and brain were added to the model. The location and size of these model organs were determined by matching their stylized shapes and locations to the corresponding CT slices. The details of these model organs are described in Table 2 and cross-sectional illustrations of their placements are shown in Fig. 2.

The organs were selected for inclusion in the stylized phantom based on biological relevance (e.g. heart, brain, ovary), tendency to accumulate ^{131}I (e.g. GI tract, liver, thyroid), or for variation from soft tissue composition (e.g. swim bladder) that would significantly impact radiation transport.

2.3.3. Voxel phantom (CSUTROUT)

There are four general steps in the procedure for creating a voxel phantom (Zaidi and Tsui, 2009; Xu and Eckerman, 2010). These include: (1) acquiring an appropriate full-body image set (such as from CT, MRI, or cryosection photography); (2) identifying and segmenting organs or other anatomical structures of interest within the image set acquired in step (1); (3) determining density and elemental composition characteristics for tissues identified in step (2); and (4) converting the organ segments (contours) to a three dimensional (3D) volume for visualization (verification of appropriate organ structure) and Monte Carlo implementation.

Table 2
Description of representative geometry for organs created in the stylized model.

Organ	Description
Body	Ellipsoid
Thyroid	18 cylindrical shells
Liver	Ellipsoid
Swim bladder	Ellipsoid, rotated 2° from horizontal
GI tract:	
Intestine	Cylinder, rotated 2° from horizontal
Cardiac stomach	Cylinder
Pyloric stomach	2 cylinders
Ovaries	2 cylinders, rotated 5° from horizontal
Heart	Ellipsoid
Brain	Sphere

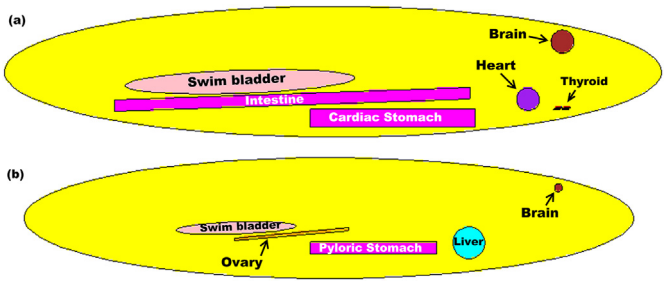

Fig. 2. Example longitudinal cross-sections of the stylized model. Cross-section (a) is through the midline of the fish body. Cross-section (b) is slightly to the lateral left (0.47 cm) of the midline of the body, and shows structures that lie behind those in (a).

Step (1), (2), and (3) were discussed above. It should be noted, however, that the thyroid was too small to be differentiated from background on CT, and was therefore contoured using knowledge of thyroid anatomy (Raine et al., 2005; Martinez et al., 2014). For step (4), once the organ contouring of step (2) was completed, the contour lines were consolidated into a 3D rendering of the two-dimensional contours, shown in Fig. 3, for visual confirmation of structure (see supplementary material online for additional figures in color).

Volumes of the contoured organs are listed in Table 3, with volumes of the organs from the stylized phantom included for comparison. It should be noted that the GI tract, as referred to in this work, consists of multiple organs: the intestine, the cardiac stomach, and the pyloric stomach, which were assigned an even distribution of the source radionuclide.

The completed set of organ contours were combined into a single boundary file using 3D-Doctor and imported into Voxelizer software, which converted the file into MCNP lattice geometry (Kramer et al., 2010). Voxelization is achieved by multiplying the pixel size (determined by image resolution) by the thickness of an image slice, converting the 2D pixels into 3D voxels (Xu and Eckerman, 2010). Voxelizer software requires minimal user input, needing only specification of boundary file dimensions and pixel size (obtained from 3D-Doctor) as well as the desired compression factor, which is a course indication of desired model resolution

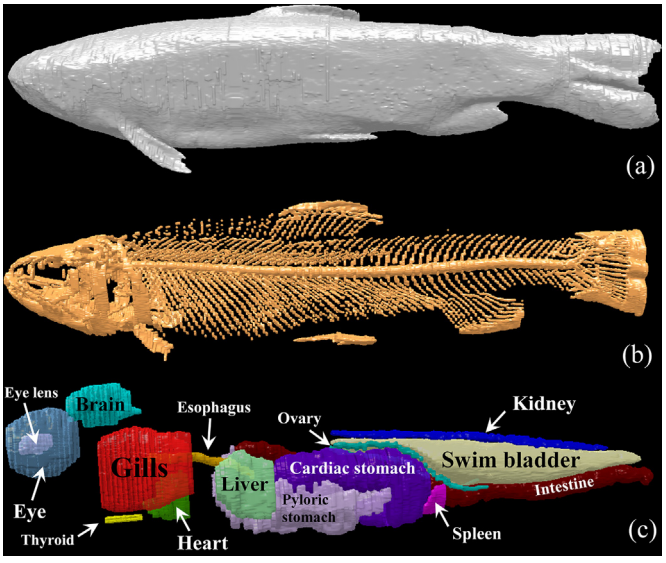

Fig. 3. Layers of the voxel phantom. From top to bottom: (a) body (b) skeleton and (c) internal organs.

Table 3
Organ volume and comparison for stylized and voxel phantoms.

Organ/organ system	Volume (cm^3)		Ratio
	Stylized phantom	Voxel phantom	
Body	212.12	208.47	1.02
Thyroid	2.4E-03	5.9E-03	0.41
Liver	0.78	0.89	0.88
Swim bladder	5.76	5.53	1.04
GI tract	9.15	8.62	1.06
Intestine	3.04	2.74	1.11
Cardiac stomach	3.69	3.34	1.11
Pyloric stomach	2.42	2.54	0.95
Esophagus	–	0.10	–
Ovaries	0.20	0.19	1.04
Heart	0.35	0.43	0.82
Brain	0.52	0.61	0.85
Spleen	–	0.07	–
Kidney	–	0.54	–
Eye (whole)	–	2.09	–
Eye lens	–	0.10	–
Gills	–	3.52	–
Bone	–	11.58	–
Remaining tissue (muscle)	186.21	165.67	1.12
		Minimum	0.41
		Median	1.03
		Maximum	1.12

native to Voxelizer software. A higher compression factor results in fewer voxels and faster computing time, but fewer voxels equate to less resolution. Compression factors of 1, 2, and 4 resulted in about 3.0×10^8, 7.5×10^7, and 1.9×10^7 voxels respectively. Because of the lengthy computing time required, a compression factor of 4 was used in this study.

As is often the convention (Xu and Eckerman, 2010), we name our phantom to distinguish it from other computational models should other researchers desire to use it (available free of charge by contacting the corresponding author); heretofore our complete voxel rainbow trout phantom will be referred to as CSUTROUT.

2.4. Source definition and determination of DCF

Within MCNP, the ^{131}I source was distributed evenly across a specific organ (i.e. the thyroid, liver, or GI tract) and disintegrations simulating decay occurred randomly across that organ. The number of disintegrations per MCNP run was chosen to minimize computing time while still achieving an acceptable relative error. The *f8 tally function in MCNP was used to tabulate the corresponding energy deposition (MeV), which was in turn normalized by disintegration prior to output (i.e. MeV dis^{-1}) (X5 Monte Carlo Team, 2003). Energy deposition was tallied for organs as well as the entire body. Separate MCNP runs were conducted for beta particles and gamma photons corresponding to ^{131}I decay, as well as for different source organs (thyroid for the simplistic model, and the thyroid, liver, and GI tract for the stylized and voxel models). The initial beta energies were randomly selected from a continuous distribution of possible energies ranging up to a maximum energy of 0.8069 MeV with an average energy of 0.1821 MeV (Stabin and CQP, 2002). Gamma energies were randomly selected from either 0.364 MeV with probability 0.817 or 0.637 MeV with probability 0.072 (Stabin and CQP, 2002). Energies deposited in the thyroid lumen (Raine et al., 2005) and the swim bladder are not included or discussed as these are non-tissue structures (within the model), containing fluid and air, respectively.

A dose conversion factor (DCF) of $0.013824 \cdot E$ mGy d^{-1} per Bq g^{-1} (where 0.013824 is a unit conversion and E is the energy deposited per disintegration (MeV dis^{-1}) in the tissue or organ of interest) was determined directly from the MCNP output.

2.5. Determination of cumulative dose rates and doses

The empirical models developed by Martinez et al. (2014) were combined with the MCNP simulation to compute cumulative organ doses from the decay of ^{131}I. First, the predicted ^{131}I concentrations (Bq kg^{-1}) in the source organ as a function of time $B(t)$, were determined from empirical models (i.e. equation (3) above). Values for a (1 Bq mL^{-1}) were chosen to normalize activity concentration by initial water concentration, and values for b (0.0862 d^{-1}) were chosen to correspond to the decay rate of ^{131}I. These values were chosen to generalize the empirical model, which assumes that the fish have no effect on ^{131}I concentration in the water. Values determined for μ and k are shown in Table 1. Concentrations of ^{131}I in the source organ were then multiplied by the appropriate mass ratio and the DCF (μGy d^{-1} per Bq kg^{-1}) obtained from MCNP to acquire a dose rate (μGy d^{-1}); the dose rate $\dot{D}(t)$, at time t is given by (4):

$$\begin{aligned}\dot{D}(t) &= \mathrm{DCF}\cdot(\text{mass ratio})\cdot B(t)\\ &= \mathrm{DCF}\cdot(\text{mass ratio})\cdot\mu\cdot\left(\frac{a}{k-b}\right)\cdot\left(e^{-b\cdot t}-e^{-k\cdot t}\right)\end{aligned} \tag{4}$$

Mass ratios were used to convert activity in the source organ to an equivalent activity for the target organ (organ for which dose is being calculated). The mass ratio will be unity in the case that the source and target organs are the same. We set the derivative of dose rate to zero, and solve for t to determine the time and magnitude of maximum dose rate:

$$\ddot{D}(t) = \mathrm{DCF}\cdot(\text{mass ratio})\cdot\mu\cdot\left(\frac{a}{k-b}\right)\cdot\left(-\mathrm{be}^{-\mathrm{bt}}+\mathrm{ke}^{-\mathrm{kt}}\right) \tag{5}$$

$$\Rightarrow t_{\max} = \frac{\ln\frac{b}{k}}{b-k} \tag{6}$$

Note that calculating the exact overall maximum dose rate (from all sources) is non-trivial and not explored here. A conservative estimation can be obtained by summing the maximum dose rates from each organ source. The dose rate was then integrated over time to determine a cumulative dose (μGy). The cumulative dose at time t, $D(t)$, is then given by (7):

$$D(t)=\mathrm{DCF}\cdot(\text{mass ratio})\cdot\mu\cdot\left(\frac{a}{k-b}\right)\cdot\left(\frac{1}{b}\left(1-e^{-\mathrm{bt}}\right)+\frac{1}{k}\left(e^{-\mathrm{kt}}-1\right)\right) \tag{7}$$

3. Results

Dose and dose rate predictions are limited to the first 32 days because the uncertainty of the extent to which the passage of ^{131}I through the food chains will continue to support the predictions beyond day 27 is unknown due to lack of data (Short et al., 1969). Values for μ and k will be constant for each phantom, as will the time to the maximum dose rate from each source organ (Tables 1 and 5 respectively). Note that once μ and k are determined, values for a and b can be varied depending on conditions of the current system. As the most significant radiation doses will be to the source organs, results are shown below for said organs as well as the whole body.

The simplistic model considers only the thyroid as a source, with no other organs surrounding it. The stylized model considers the same thyroid and fish body as the simplistic model, with eight additional organs. CSUTROUT consists of a three-dimensional rendering of an actual fish body, and includes the same organs as the stylized model, with seven additional organs. The stylized model and CSUTROUT both consider ^{131}I uptake in the thyroid, liver,

Table 4
Summary of maximum dose rates and cumulative 32 day doses to the whole body, thyroid, liver, and GI tract. Doses and dose rates are listed by source organ (i.e. for CSUTROUT, the maximum dose rate to the whole body from ^{131}I in the thyroid is 3.7E-02 μGy d^{-1}) and assume an initial water concentration of 1 Bq mL^{-1}.

Model	Maximum dose rate (μGy d^{-1}) by source organ				Cumulative 32 day dose (μGy) by source organ			
	Thyroid	Liver	GI Tract	Total (approx.)	Thyroid	Liver	GI Tract	Total
Time to $\dot{D}_{max}$	*19.43 d*	*22.03 d*	*14.78 d*					
Simplistic								
Whole body	2.9E-02	–	–	7.6E-01	7.6E-01	–	–	7.6E-01
Thyroid	4.7E+02	–	–	1.2E+04	1.2E+04	–	–	1.2E+04
Stylized								
Whole body	2.9E-02	3.1E-01	5.0E+00	5.3E+00	7.6E-01	8.1E+00	1.3E+02	1.4E+02
Thyroid	4.7E+02	1.6E-02	4.7E-02	4.7E+02	1.2E+04	4.2E-01	1.2E+00	1.2E+04
Liver	1.6E-03	7.4E+01	7.6E-01	7.4E+01	4.2E-02	1.9E+03	1.9E+01	1.9E+03
GI tract	3.7E-04	4.8E-02	1.0E+02	1.0E+02	9.6E-03	1.2E+00	2.6E+03	2.6E+03
CSUTROUT								
Whole body	3.7E-02	3.8E-01	5.0E+00	5.4E+00	9.7E-01	9.9E+00	1.3E+02	1.4E+02
Thyroid	6.2E+02	4.2E-02	2.1E-01	6.2E+02	1.6E+04	1.1E+00	5.4E+00	1.6E+04
Liver	5.5E-03	7.2E+01	2.3E+00	7.5E+01	1.4E-01	1.9E+03	5.9E+01	1.9E+03
GI tract	2.0E-03	1.8E-01	9.7E+01	9.7E+01	5.3E-02	4.7E+00	2.5E+03	2.5E+03

and the GI tract. The maximum dose rates and cumulative doses for source organs and whole body are listed in Table 4 for each model. Fig. 4 illustrates model comparison of cumulative doses received to source organs considered in the stylized model and CSUTROUT. Absolute differences in cumulative dose corresponding to Fig. 4, along with percentage differences, are listed in Table 5. Results for DCFs as well as details of cumulative doses and dose rates received to all organs are contained in online supplementary material.

4. Discussion

4.1. Current limitations

To ensure adequate sampling of thyroid tissue, most studies, including Short et al. (1969), removed tissue from the mandible area that contained both thyroid and non-thyroid tissue. These samples were described as “thyroid area” samples, and the concentration of ^{131}I in these “thyroid area” samples likely underestimated the ^{131}I concentrations of the true thyroid tissues, which would cause radiation doses determined here to also be underestimated.

Additionally, the GI tract is modeled as a solid organ (consistent with previous work, e.g. Ruedig et al., 2014) with a homogenous source distribution. Gut contents will not be the same composition as GI tissue, but the exact composition at this point is unknown. Detailed elemental composition for gut contents as well as fish tissues calls for further investigation. Also, the pyloric stomach consists of a number of small, finger-like tubes called caeca (Weinreb and Bilstad, 1955). The pyloric caeca were not contoured individually as they were not discernable from the gut contents on CT, which may alter results slightly (please see supplementary online material for an internal anatomy image for the trout considered here as well as example cross-sections of organ contours used to develop CSUTROUT.)

Often, as with Short et al. (1969), studies do not specify if gut contents were included in reported activity concentrations for the GI tract, although radiation dose will depend on how the activity is distributed within the GI tract. Activity contained in the gut contents will contribute to the radiation dose received by the GI tract epithelial tissue, but some of the radiation may be attenuated (i.e. some energy will be deposited in the gut contents rather than in tissue). The volume of gut contents is quite variable, and the volume of GI tract epithelial tissue can potentially be much less than total volume of the GI tract. The extent of the variation, and the subsequent effect on results, is not explored here, but certainly warrants further investigation.

4.2. General considerations

MCNP presents a relative error (at the 1σ level) corresponding to the precision of the MCNP calculation along with the tally result (MeV dis^{-1}). Results with a relative error <0.10 can generally be considered reliable (X-5 Monte Carlo Team, 2003). Results presented here for whole body and source organs are all associated with relative errors <0.01, with most <0.001. However, for organs assumed to not contain ^{131}I, relative errors are higher; relative error will increase (1) as distance from the source increases and (2) as volume of an organ decreases. Fewer particles depositing energy in an organ will weaken the statistics associated with that organ, occasionally resulting in large relative errors. The few relative errors >0.10 were generally <0.50 (hence within a factor of a few; X-5 Monte Carlo Team, 2003) and associated with doses insignificant when compared to the contribution from another source. For our purposes it was not considered worthwhile to reduce these errors

Table 5
Cumulative dose comparison. Absolute differences (Abs) in 32 day cumulative absorbed dose (μGy) along with percentage differences (%) between the stylized model and CSUTROUT predictions for dose to the whole body, thyroid, liver, and GI tract. Values for self-contribution (e.g. differences in dose to the thyroid from the thyroid) are shown in bold.

	Absolute (μGy) and percentage differences between models by source organ							
	Thyroid		Liver		GI Tract		Overall	
	Abs	%	Abs	%	Abs (μGy)	%	Abs (μGy)	%
Whole body	2.0E-01	24	1.7E+00	19	8.3E-01	0.7	1.1E+00	0.8
Thyroid	**4.0E+03**	**28**	6.8E-01	110	4.2E+00	151	4.0E+03	28
Liver	1.0E-01	108	**3.5E+01**	**1.9**	4.0E+01	102	5.0E+00	0.3
GI Tract	4.3E-02	138	3.5E+00	117	**1.2E+02**	**4.8**	1.2E+02	4.7

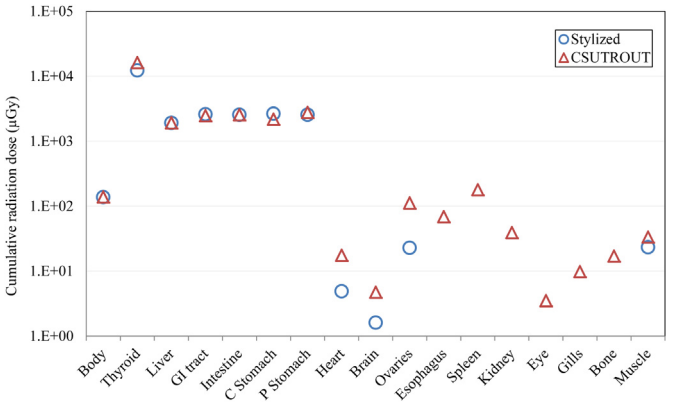

Fig. 4. Comparison of total radiation dose. Cumulative 32 day radiation dose from ^{131}I (log scale) received by organs in the stylized model and in CSUTROUT from all three of the internal source organs (thyroid, liver, and GI tract).

further, given the considerable run-time required to do so. The objective of this paper is to present and apply a methodology for calculating dose using different phantom types; if a dose-effects study focused on a specific organ was to be undertaken, the MCNP code should be refined to focus on precise results for the organ(s) of concern.

Although we consider three source organs here, in reality, iodine will be found throughout the body. Any area containing ^{131}I will have an increased dose and dose rate, with a corresponding increase in risk of deleterious effects due to radiation exposure. For example, although Short et al. (1969, 1971) did not sample trout ovary, intraperitoneal injections of ^{131}I in channel catfish (*Ictalurus punctatus*) have shown that a majority of the injected ^{131}I can accumulate in the ovaries (Lindsay et al., 1969; Tarrant, 1971). Corresponding ^{131}I injection studies are absent for the rainbow trout, although similar accumulations of stable iodine in ovaries occurs for this species in freshwater (Robertson and Chaney, 1953). Robertson and Chaney (1953) report that more than 50% of all the fish's stable iodine occurs in the eggs of a reproductively active female rainbow trout. The potential concentration of ^{131}I in ovaries following an accidental release during a fish's reproductively active period suggests the potential for mutagenic effects and impacts on succeeding generations, although the comparative radiosensitivity of thyroid and egg tissues appears to be undocumented.

4.3. Model comparison

Progressively more detailed phantoms were considered to assess the difference in organ dose and DCFs with improved anatomical realism. The results for the thyroid and whole body (considering only the thyroid as a source organ) were the same for the simplistic and stylized model, meaning that prior to the consideration of additional source organs, the change in body composition utilized by the stylized model had insignificant effect on thyroid dose. Note, however, that the GI tract was the greatest contributor to whole body dose. Although the GI tract had lower activity concentration than the thyroid, the total activity within the organ was higher. Because the stylized model is more robust than the simplistic, we consider only the differences in the stylized phantom and CSUTROUT for organs the models have in common.

4.3.1. Cumulative 32 day dose

The models are similar in prediction of dose, especially for source organs. Organs not containing ^{131}I generally had much higher percentage differences between the models, but relatively small absolute differences (similar to source organ dose contributions from other organs, e.g. dose to the GI tract from the liver). The thyroid received the highest doses (1.23×10^4 and 1.63×10^4 μGy, stylized model and CSUTROUT respectively), due to preferential uptake of ^{131}I. The highest doses to organs not containing ^{131}I were the ovaries (2.28×10^1 and 1.13×10^2 μGy using the stylized model and CSUTROUT respectively) and the spleen (1.79×10^2 μGy, CSUTROUT), although these doses were much lower than doses to the source organs (between 1.9×10^3 and 1.63×10^4 μGy). The highest doses to these organs were due to radiation exposure from the GI tract; the GI tract is a larger organ system than either the liver or thyroid and lies in close proximity to several other organs, meaning a radiation source distributed in the GI tract will have a wider distribution and, in general, a shorter path to other organs. The distance between an organ and the source organ is particularly relevant for ^{131}I as beta particles have a relatively short range (Cember and Johnson, 2009).

The larger percent differences for ^{131}I distributed in the thyroid are equated to the difference in size between the thyroid organs of the stylized model and CSUTROUT. The thyroid in CSUTROUT was not visible on CT and had to be approximated by hand, and although the absolute difference between thyroid sizes in the stylized and CSUTROUT model is only 3.5 mm^3, the CSUTROUT thyroid (only 13 voxels) is ~2.5X the size of the stylized thyroid, which is more anatomically correct (Raine et al., 2005).

4.3.2. Difference between direct calculation and using mass ratios to determine organ dose

Organ dose (or similarly dose rate) and DCF (by extension) can be related to the corresponding whole body values by equation (8) (Gómez-Ros et al., 2008) and (9) respectively:

$$D_{\text{organ}} = D_{\text{whole body}} \left(\frac{\text{AF}_{\text{organ}}}{\text{AF}_{\text{whole body}}} \right) \left(\frac{m_{\text{whole body}}}{m_{\text{organ}}} \right) \tag{8}$$

$$\text{DCF}_{\text{organ}} = \text{DCF}_{\text{whole body}} \left(\frac{\text{AF}_{\text{organ}}}{\text{AF}_{\text{whole body}}} \right) \tag{9}$$

where AF is the absorbed fraction, or the proportion of energy emitted and absorbed in the organ or whole body as specified. In the absence of organ-specific data, a conservative estimate of organ dose can be determined by (10):

$$D_{\text{organ}} = D_{\text{whole body}} \left(\frac{m_{\text{whole body}}}{m_{\text{organ}}} \right) \tag{10}$$

as the maximum value for the absorbed fraction quotient in (8) and (9) is 1 (Gómez-Ros et al., 2008). A conservative estimate of organ-specific DCF would therefore be the whole body DCF. It should be noted that the mass ratio approach discussed here is only valid for source organs; that is, the assumption when applying equation (10) is that the source resulting in $D_{\text{whole body}}$ is contained within the organ for which D_{organ} is being calculated (Gómez-Ros et al., 2008). Organ doses were calculated directly from MCNP output and then calculated again using the mass ratio approach. Separate calculations were done for each individual source organ. The factor difference (ratio) between these two values is shown in Fig. 5; note that this factor difference is equivalent to $\text{AF}_{\text{whole body}}/\text{AF}_{\text{organ}}$ and $\text{DCF}_{\text{whole body}}/\text{DCF}_{\text{organ}}$, as follows from (9) and the ratio of (10) to (8). The GI tract is included as a whole without inclusion of the intestine and stomachs. The intestine and stomachs combine to form the source contributing to the dose received by the whole body, so the mass ratio approach applied individually would provide an inflated result.

All factor differences are less than 10, with the liver and GI tract having factor differences very close to unity. The differences between models are due to the slight difference in size and location of the particular organs, although these differences are small. The thyroid has the largest difference due to the relative size difference between models. Generally, the larger the mass ratio the larger the difference will be between the predicted and actual doses, which is illustrated here in the case of the thyroid modelling differences (the larger thyroid resulted in a smaller difference). The mass ratio approach is therefore a generally reasonable approximation of organ dose, given the simplified assumptions of this and the Gómez-Ros et al. (2008) models.

4.4. Consideration of fish size using the simplistic model

We consider the simplistic model in comparing size effect on the ability of the mass ratio method to predict dose to the thyroid. The thyroid has the greatest difference between the mass ratio method and the direct method for dose approximation (out of the three source organs; Fig. 5). CSUTROUT cannot be resized, so cannot be used for assessing differences in fish size. The DCFs determined by the stylized and simplistic models (with the thyroid as the source organ) are the same; therefore we use the previously scaled set of simple models developed in Martinez et al. (2014), along with the simplistic model used here, to consider the difference fish size will have on the mass ratio prediction of organ radiation dose (or organ dose conversion factors).

Consider the energy deposition distribution shown in Fig. 6. More energy will be proportionally deposited in the thyroid of a larger fish than in a smaller fish (Table 6 contains specifications of fish dimensions). The probability of interactions between beta or gamma radiations and the media through which they travel (e.g. tissue) increases with distance travelled. Also, in addition to having a relatively short range, beta particles will deposit most of their energy towards the end of their range, just prior to coming to a stop (Cember and Johnson, 2009). As fish size increased, a larger proportion of energy was deposited in the thyroid per unit mass. More energy was deposited in the larger fish thyroid per unit mass due to larger tubule sheath dimensions. Juvenile fish with tubule sheath thickness of 10 μm (Martinez et al., 2014) will result in radiation readily passing through the thyroid tissues and depositing minimal energy. Increasing the thickness of the tubule sheaths in the larger fish increases the likelihood (e.g. frequency) of radiation–tissue interactions.

Because of the differences in relative energy deposition between different fish sizes, DCF for the thyroid and for the whole body will be different. Values for DCFs of the different size simplistic models are shown in Table 6. However, the mass ratios (whole body to thyroid) remain the same. The mass ratio method for estimating thyroid organ dose will therefore give proportionally different results for different size fish. The estimated thyroid radiation dose as calculated by each method, for each size fish, is shown in Table 6, along with the ratio between them.

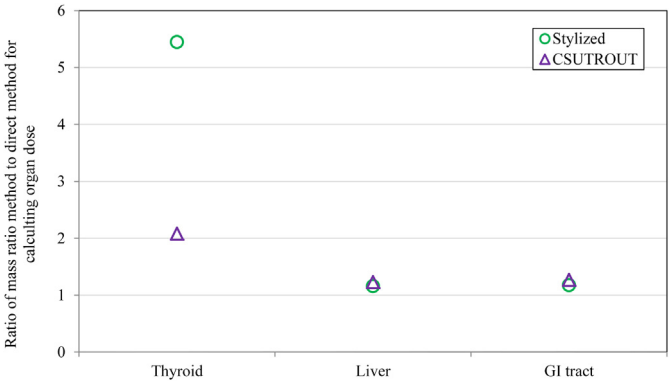

Fig. 5. Differences in methods for calculating organ dose. The factor difference between calculating thyroid dose directly and by using the mass ratio approach is shown for both the stylized phantom and CSUTROUT.

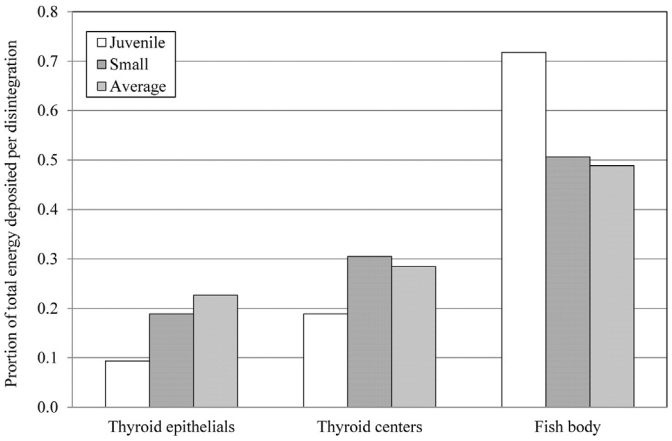

Fig. 6. Energy distribution by organ and fish size. The proportion of energy deposited in the thyroid epithelial, thyroid lumen, and fish body (other than the thyroid) for three different sizes of fish; data from Martinez et al. (2014).

The mass ratio method becomes more accurate as fish size increases because the absorbed fraction quotient between organ and whole body increases. The relationship between fish size and relative accuracy of the mass ratio approach is shown graphically in Fig. 7. This figure further demonstrates that the mass ratio approach is indeed a valid approximation of organ radiation dose, as suggested by Gómez-Ros et al. (2008). The larger the animal and organs, the more accurate the mass ratio approach, as larger organs will self-absorb more radiation than smaller organs, especially for low penetrating radiation (e.g. beta radiation).

4.5. Model development and utility considerations

Although the voxel phantom provides the most anatomically accurate model, the development process is very time-consuming. Automatic segmentation is an available feature of 3D-Doctor, but cannot adequately distinguish the various soft tissue organs.

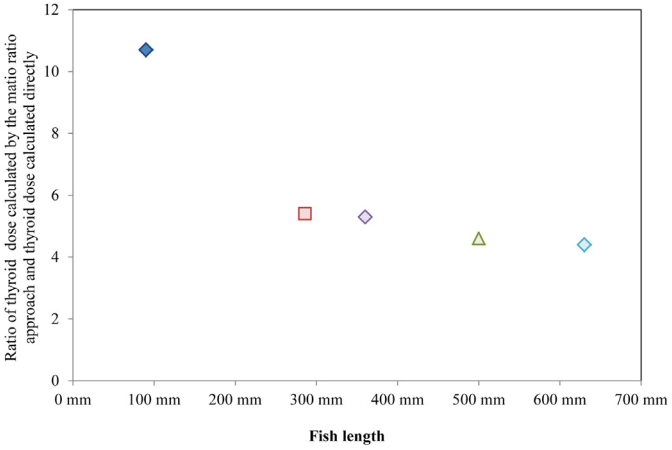

Fig. 7. Ratio of indirect to direct method for calculation of organ dose. Graphical illustration of the ratio of estimated radiation thyroid dose determined by (1) converting the whole body dose to thyroid dose using mass ratios and (2) calculating the thyroid dose directly for trout of 5 different lengths. Diamonds represent body ratios (length:height:width) of 9:2:1. The square and triangle represent alternate body dimensions as discussed in the text.

Table 6
Dose conversion factors and estimated cumulative 32 day thyroid radiation dose for different fish sizes, assuming ^{131}I contained in the thyroid. Fish size and corresponding dose conversion factors for both the thyroid epithelial and whole body[a] along with cumulative thyroid radiation dose as determined directly (using the thyroid DCF) and indirectly (using mass ratios) for different size fish, with the ratio between the two approximations.

Fish reference	Fish size (length, mass)	DCF (μGy d^{-1} kg Bq^{-1})		Cumulative thyroid radiation dose (mGy)		Ratio
		Thyroid epithelial	Total body	Using thyroid DCF	Using mass ratios	
Juvenile	90 mm, 9.896 g	2.7E-04	2.8E-03	5.9	63.2	10.7
Current study	286 mm, 222.7 g	5.4E-04	3.0E-03	12.3	67.1	5.4
Small	360 mm, 633.3 g	6.1E-04	3.2E-03	13.5	71.6	5.3
ICRP[b]	500 mm, 1257 g	7.2E-04	3.3E-03	16.1	74.2	4.6
Average	630 mm, 3394 g	8.1E-04	3.6E-03	18.0	79.6	4.4

[a] The juvenile, small, and average fish all have relative dimensions of 9:2:1 (length:width:height), scaled from data in Raine et al. (2005). The simplistic model developed here has a length:width:height of about 11.5:2.3:1, and the ICRP representation developed in Martinez et al. (2014) study (adding the thyroid) has a length:width:height of about 8.3:1.3: 1. However, thyroid dimensions (all) were determined relative to the length of the fish.

[b] The ICRP representation for reference trout listed here and developed in Martinez et al. (2014) uses a soft tissue density of 1 g cm^3 to correspond with that listed in ICRP 108 (ICRP, 2008). Soft tissue in the other models was assigned a density of 1.05 g cm^3 to be consistent with ICRU tissue compositions (ICRU, 1989).

Manual contouring of organs on the original image set is labor-intensive, tedious, and involves user-specific assumptions about anatomy. Additionally, several organs have very low image contrast, making the segmentation nearly impossible, and other organs, such as the fish thyroid, are so small as to be beyond the resolution of the CT image slices. For organ dose calculations numerous internal organs/tissues have to be identified and contoured, and the resulting size of a whole-body computational phantom with organs can potentially be too large for MCNP to process (Xu and Eckerman, 2010). The compression factor of the boundary file (organ contours) can be changed to reduce the number of voxels, but resolution is sacrificed. Whereas stylized phantoms can be easily scaled to different sizes (Martinez et al., 2014), the voxel phantom developed here is fish specific. Different species, sizes, life stages, and sex will require a different voxel phantom be developed for the most accurate dose assessment. These issues are consistent with voxel phantom development in general (Xu and Eckerman, 2010).

5. Conclusions

5.1. Model refinements

Although the models presented here provide greater dosimetric accuracy and flexibility than the traditional homogenous ellipsoids, some limitations remain. The extent to which tissue and gut content elemental composition will impact the results reported here is currently unknown, and warrants further investigation (currently in progress). Greater sampling precision will improve the accuracy of both the empirical model (thyroid) and computational model (GI tract) when developing future models. A higher resolution image set (such as obtained by microCT) used to create the voxel phantom will improve anatomical accuracy, although as the stylized phantom and CSUTROUT provided similar results, the added benefit of such increased accuracy is not clear.

5.2. Consideration of the mass ratio approach

Although calculations in this study did not assume a homogenous whole body distribution of radionuclides (as ICRP, ERICA, and Gómez-Ros et al., 2008), using the mass ratio approach (considering three source organs individually) was a reasonable approximation for calculating organ dose. However, the mass ratio approach is only valid for organs with preferential uptake of a radionuclide, and cannot account for contributions from multiple source organs. Therefore, one significant benefit of both the stylized phantom and CSUTROUT is the ability to consider multiple source organs when determining radiation dose, along with the ability to determine dose in organs due to “cross fire,” i.e. the ability to calculate dose to organs from other organs (Ruedig et al., 2014).

5.3. Optimal phantom choice

Although CSUTROUT was the most anatomically realistic phantom, it required much more resource dedication to develop than did the stylized phantom for similar results. Additionally, the stylized phantom can be scaled to represent trout sizes whereas CSUTROUT cannot. There may be instances where a detailed phantom such as CSUTROUT is appropriate, as it will provide the most accurate radiation dose and dose rate information for the size, sex, and species considered, but generally, the stylized phantom appears to be the best choice for an ideal balance between accuracy and resource requirements.

5.4. Utility and future implications of model development

The results of this study work towards eventual application and integration into the regulatory paradigm of environmental protection of non-human biota. For example, either model (stylized or CSUTROUT) could be used in demonstrating regulatory compliance in environmental protection. This would be especially relevant in a situation where an activity does not fall within the conservative bounds of the ICRP's ellipsoidal models, but may still be within protective dose limits.

Experiments conducted to determine specific radiation effects to fish (such as those seen by La Roche et al., 1966) can be supplemented with the models developed here to equate effects with certain doses or dose rates. In addition to establishing environmental benchmarks of health, relating radiation dose to the effects of radiological contaminants in organisms and ecosystems has applications in emergency response and recovery as well as resource management. The combination of computational and empirical models described here could be used for any radionuclide, with available data, to determine activity concentrations and radiation doses to fish, and similar methodology can be used to develop appropriate models for any species. If the loss rate is assumed to correspond to ^{131}I decay, the initial water concentration immediately after an accidental release is the only piece of information needed to approximate maximum dose rates to a freshwater fish of similar size to the models developed here (see Martinez et al., 2014 for application to the Kiev Reservoir after the Chernobyl release). Once the dose level at which effects are seen is established, the dosimetric methodology presented here will enable rapid determination of whether or not adverse effects

are to be expected. Knowledge of the impact of an accidental or purposeful release of radiation would have specific and beneficial utility for fisheries, for fishing communities, and for general assessment and protection of aquatic environment health.

Acknowledgements

N Martinez was supported in part by the CDC/NIOSH Mountain & Plains Educational and Research Center (NIOSH grant number: T42 OH009229-06). The contents herein, however, are solely the responsibility of the author and do not represent the official views of the CDC, NIOSH and MAP ERC.

Appendix A. Supplementary data

Supplementary data associated with this article can be found, in the online version, at http://dx.doi.org/10.1016/j.jenvrad.2014.08.001.

References

Bird, G.A., Motycka, M., Rosentreter, J., Schwartz, W.J., Vilks, P., 1995a. Behavior of ^{125}I added to limnocorrals in two Canadian shield lakes of different trophic states. Sci. Total Environ. 166, 161–177.
Bird, G.A., Schwartz, W.J., Rosentreter, J., 1995b. Evolution of ^{131}I from freshwater and its partitioning in simple aquatic microcosms. Sci. Total Environ. 164, 151–159.
Bird, G.A., Schwartz, W.J., 1996. Distribution coefficients, K_ds, for iodine in Canadian shield lake sediments under oxic and anoxic conditions. J. Environ. Radioact. 35, 261279.
Bitar, A., Lisbona, A., Thedrez, P., Maurel, C.S., Le Forestier, D., Barbet, J., Bardies, M., 2007. A voxel-based mouse for internal dose calculations using Monte Carlo simulations (MCNP). Phys. Med. Biology 52, 1013–1025.
Caffrey, E.A., Higley, K.A., 2013. Creation of a voxel phantom of the ICRP reference crab. J. Environ. Radioact. 120, 14–18.
Cember, H., Johnson, T.E., 2009. Introduction to Health Physics. McGraw-Hill, New York.
Diem, K., Lentner, C. (Eds.), 1970. Scientific Tables, seventh ed. GEIGY Pharmaceuticals, Ardsley.
Dogdas, B., Stout, D., Chatziioannou, A.F., Leahy, R.M., 2007. Digimouse: a 3D whole body mouse atlas from CT and cryosection data. Phys. Med. Biol. 52, 577–587.
Donaldson, L.R., Olson, P.R., Donaldson, J.R., 1959. The Fern Lake trace mineral metabolism program. Trans. Am. Fish. Soc. 88, 1–6.
Gilfedder, B.S., Petri, M., Biester, H., 2009. Iodine speciation and cycling in fresh waters a case study from a humic rich headwater lake (Mummelsee). J. Limnol. 68, 396–408.
Gilfedder, B.S., Petri, M., Wessels, M., Biester, H., 2010. An iodine mass-balance for Lake Constance, Germany insights into iodine speciation changes and fluxes. Geochimica et Cosmochimica Acta 74, 3090–3111.
Gómez-Ros, J.M., Prohl, G., Ulanovsky, A., Lis, M., 2008. Uncertainties of internal dose assessment for animals and plants due to non-homogeneously distributed radionuclides. J. Environ. Radioact. 99, 1449–1455.
Hindorf, C., Ljungberg, M., Strand, S.E., 2004. Evaluation of parameters influencing S values in mouse dosimetry. J. Nucl. Med. 45, 1950–1960.
ICRP, 2008. Environmental Protection the Concept and Use of Reference Animals and Plants. ICRP Publication 108. Elsevier, Oxford.
ICRU, 1989. Tissue Substitution in Radiation Dosimetry and Measurement. ICRU Report 44. ICRU, Bethesda.
Kinase, S., 2008. Voxel-based frog phantom for internal dose evaluation. J. Nucl. Sci. Technol. 45, 1049–1052.
Kramer, G.H., Capello, K., Chiang, A., Cardenas-Mendez, E., Sabourin, T., 2010. Tools for creating and manipulating voxel phantoms. Health Phys. 98, 542–548.
Kramer, G.H., Capello, K., Strocchi, S., Bearrs, B., Leung, K., Martinez, N., 2012. The HML's new voxel phantoms two human males, one human female, and two male canines. Health Phys. 103, 802–807.
La Roche, G., Johnson, C.L., Woodall, A.N., 1965. Thyroid function in the rainbow trout (Salmo gairdneri, Rich): I. Biochemical and histological evidence of radiothyroidectomy. General. Comp. Endocrinol. 5, 145–159.
La Roche, G., Woodall, A.N., Johnson, C.L., Halver, J.E., 1966. Thyroid function in the rainbow trout (*Salmo gairdneri*, Rich): II. Effects of thyroidectomy on the development of young fish. General. Comp. Endocrinol. 6, 249–266.
Larsson, C.M., 2008. An overview of the ERICA integrated approach to the assessment and management of environmental risks from ionising contaminants. J. Environ. Radioact. 99, 1364–1370.
Lindsay, R.H., Romine, C., Zacharewicz, F., Dupree, H.K., Sneed, K.E., 1966. Accumulation of ^{131}I by channel catfish (*Ictalurus punctatus*) ovaries in vivo and in vitro. General. Comp. Endrocrinol. 6, 231–238.
Martinez, N.E., Johnson, T.E., Pinder 3rd, J.E., 2014. Influence of lake trophic structure on ^{131}I accumulation and subsequent cumulative radiation dose to trout thyroids. J. Environ. Radioact. 131, 62–71.
Mauxion, T., Barbet, J., Suhard, J., Pouget, J.P., Poirot, M., Bardies, M., 2013. Improved realism of hybrid mouse models may not be sufficient to generate reference dosimetric data. Med. Phys. 40, 052501.
Mohammadi, A., Kinase, S., Saito, K., 2011. Comparison of photon and electron absorbed fractions in voxel-based and simplified phantoms for small animals. Prog. Nucl. Sci. Technol. 2, 365–368.
Mohammadi, A., Kinase, S., Saito, K., 2012. Evaluation of absorbed doses in voxel-based and simplified models for small animals. Radiat. Prot. Dosim. 150, 283–291.
Olsen, S., Chakravarti, D., Olson, P.R., 1967. Water, bottom deposits, and zooplankton of Fern Lake. Wash. Limnol. Oceanogr. 12, 392–404.
Padilla, L., Lee, C., Milner, R., Shahlaee, A., Bolch, W., 2008. Canine anatomic phantom for preclinical dosimetry in internal emitter therapy. J. Nucl. Med. 49, 46–452.
Pinder III, J.E., Hinton, T.G., Whicker, F.W., Smith, J.T., 2009. Cesium accumulation by Fish.fish following acute input to lakes: a comparison of experimental and Chernobyl-impacted systems. J. Environ. Radioact. 100, 456–467.
Pinder III, J.E., Hinton, T.G., Taylor, B.T., Whicker, F.W., 2011. Cesium accumulation by aquatic organisms at different trophic levels following an experimental release into a small reservoir. J. Environ. Radioact. 102, 283–293.
Raine, J.C., Strelive, U., Leatherland, J.F., 2005. The thyroid tissue of juvenile *Oncorhynchus mykiss* is tubular, not follicular. J. Fish. Biol. 67, 823–833.
Robertson, O.H., Chaney, A.L., 1953. Thyroid hyperplasia and tissue iodine content in spawning rainbow trout: a comparative study of Lake Michigan and California sea-run trout. Physiol. Zool. 26, 328–340.
Ruedig, E., Caffrey, E., Hess, C., Higley, H., 2014. Monte Carlo derived absorbed fractions for a voxelized model of *Oncorhynchus mykiss*, a rainbow trout. Radiat. Environ. Biophyis. 53, 581–587.
Segars, W.P., Tsui, B.M., Frey, E.C., Johnson, G.A., Berr, S.S., 2004. Development of a 4-D digital mouse phantom for molecular imaging research. Mol. Imaging Biol. 6, 149–159.
Short, Z.F., Palumbo, R.F., Olson, P.R., Donaldson, J.R., 1969. The uptake of ^{131}I by the biota of Fern Lake, Washington, in a laboratory and a field experiment. Ecology 50, 1979–1989.
Short, Z.F., Olson, P.R., Palumbo, R.F., Donaldson, J.R., Lowman, F.G., 1971. Uptake of molybdenum, marked with ^{99}Mo, by the biota of Fern Lake, Washington, in a laboratory and a field experiment. In: Proceedings of the Third National Symposium on Radioecology, vol. 1 (Oak Ridge, TN).
Smith, J.T., Kudelsky, A.V., Ryabov, I.N., Daire, S.E., Boyer, L., Blust, R.J., Fernandez, J.A., Hadderingh, R.H., 2002. Uptake and elimination of radiocesium in fish and the "size effect". J. Environ. Radioact. 62, 145–164.
Stabin, M.G., da Luz L, C.Q.P., 2002. Decay energy for internal and external dose assessment. Health Phys. 83, 471–475.
Stabin, M.G., Peterson, T.E., Holburn, G.E., Emmons, M.A., 2006. Voxel-based mouse and rat models for internal dose calculations. J. Nucl. Med. 47, 655–659.
Tarrant Jr., R.M., 1971. Seasonal variation in the accumulation and loss of ^{131}I by tissues of adult female channel catfish, *Ictalurus punctatus* (Rafinesque). Trans. Am. Fish. Soc. 100, 237–246.
Taschereau, R., Chow, P.L., Chatziioannou, A.F., 2006. Monte Carlo simulations of dose from microCT imaging procedures in a realistic mouse phantom. Med. Phys. 33, 216–224.
Weinreb, E.L., Bilstad, N.M., 1955. Histology of the digestive tract and adjacent structures of the Rainbow Trout. Salmo Gairdneri irideus Copeia 3, 194–204.
Whicker, F.W., Schultz, V., 1982. Radioecology: Nuclear Energy and the Environment Volume 2. CRC Press Inc, Boca Raton.
Wu, L., Zhang, G., Luo, Q., Liu, Q., 2008. An image-based rat model for Monte Carlo organ dose calculations. Med. Phys. 35, 3759–3764.
X-5 Monte Carlo Team, 2003. MCNP – a General N-particle Transportation Code, Version 5 Volume 1 Overview and Theory. Los Alamos National Laboratory Report LA-UR 31987 (Los Alamos, NM).
Xie, T., Zhang, G., Li, Y., Liu, Q., 2010a. Comparison of absorbed fractions of electrons and photons using three kinds of computational phantoms of rat. Appl. Phys. Lett. 97, 1–3.
Xie, T., Han, D., Liu, Y., Sun, W., Liu, Q., 2010b. Skeletal dosimetry in a voxel-based rat phantom for internal exposures to photons and electrons. Med. Phys. 37, 2167–2178.
Xu, X.G., Eckerman, K.F. (Eds.), 2010. Handbook of Anatomical Models for Radiation Dosimetry. Taylor and Francis, Group Boca Raton.
Zaidi, H., Tsui, B.M.W., 2009. Review of computational anthropomorphic anatomical and physiological models. Proc. IEEE 97, 1938–1953.
Zhang, G., Xie, T., Bosmans, H., Liu, Q., 2009. Development of a rat computational phantom using boundary representation method for Monte Carlo simulation in radiological imaging. Proc. IEEE 97, 2006–2014.
Zhang, X., Ziangdong, X., Cheng, J., Ning, J., Yuan, Y., Yang, G., 2012. Organ dose conversion coefficients based on a voxel mouse model and MCNP code for external photon irradiation. Radiat. Prot. Dosim. 148, 9–19.